Table of Contents

1) Experimental details

Synthesis. The catalysts were prepared by co-impregnation using aqueous metal nitrate solutions followed by calcination in air at 623 K for 2h resulting in the calcined catalyst precursors Rh-Mn-Fe/SiO_2 (ID 21102), Rh-Mn/SiO_2 (ID 20818), Rh- Fe/SiO_2 (ID 22436), Rh/SiO_2 (ID 21104), Mn/SiO_2 (ID 20508), and Fe/SiO_2 (ID 21103). Davisil 636, 250-500 µm (ID 20510) was used as support.

Reduction procedure. The reduction of the calcined Rh-based catalysts was performed in a quartz tube under atmospheric pressure using a gas mixture of 5 vol% H_2 in argon at a flow rate of 50 ml/min. The samples were heated and held at 350°C for 1 h with a rate of 5 K/min followed by subsequent cooling to room temperature. In another case, the Rh-Mn-Fe/SiO_2 catalyst was reduced at 350°C for 4 h in gas mixture of 5%H_2/Ar. This sample was not exposed to air during TEM sample preparation and transferred from glove box to the machine.

TEM characterization. TEM samples were prepared by drop casting a few drops of suspensions on Cu TEM grids and were dried naturally in the air. For the Rh-Mn-Fe/SiO2 catalyst reduced for 4h in H_2/Ar, the TEM sample was dry-prepared in a glove box and transferred to the TEM machine by a vacuum transfer holder (Gatan) without air contact during the process. HAADF-STEM images, EDX-Maps, and STEM-EELS and maps were taken on an abreaction-corrected JEOL JEM-ARM200F TEM equipped with a high angle Silicon Drift EDX detector with a detection area of 100mm2 and a GIF Quantum energy filter. Dual EELS mode was applied to record spontaneously the low loss and high loss spectra.

XPS measurement. All samples were measured as pressed pellets. The reduced catalysts were transferred without air contact into a glove box attached to the spectrometer transfer system. Spectra were recorded at room temperature, using non-monochromatized Al Kα (1486.6 eV) excitation and a hemispherical analyzer (Phoibos 150, SPECS). The binding energy scale was calibrated by the standard Au4f(7/2) and Cu2p(3/2) procedure and correction for charging effects was carried out by internal referencing the Si2p(3/2) line to literature values of SiO_2 (103.3 eV).[48] Charging was ~5.0 eV (4.75-5.1 eV).

Catalytic test. The catalysts were tested in CO hydrogenation under varying reaction conditions. The data shown in Figure. S1 (a-b) refer to reference conditions (260 °C, 54 bar, 60% H_2, 20% CO, N_2 balance, 2917 h^{-1}) repeatedly tested within the experimental program.

2) Catalytic performances of Rh-Mn/SiO_2 and Rh-Mn-Fe/SiO_2.

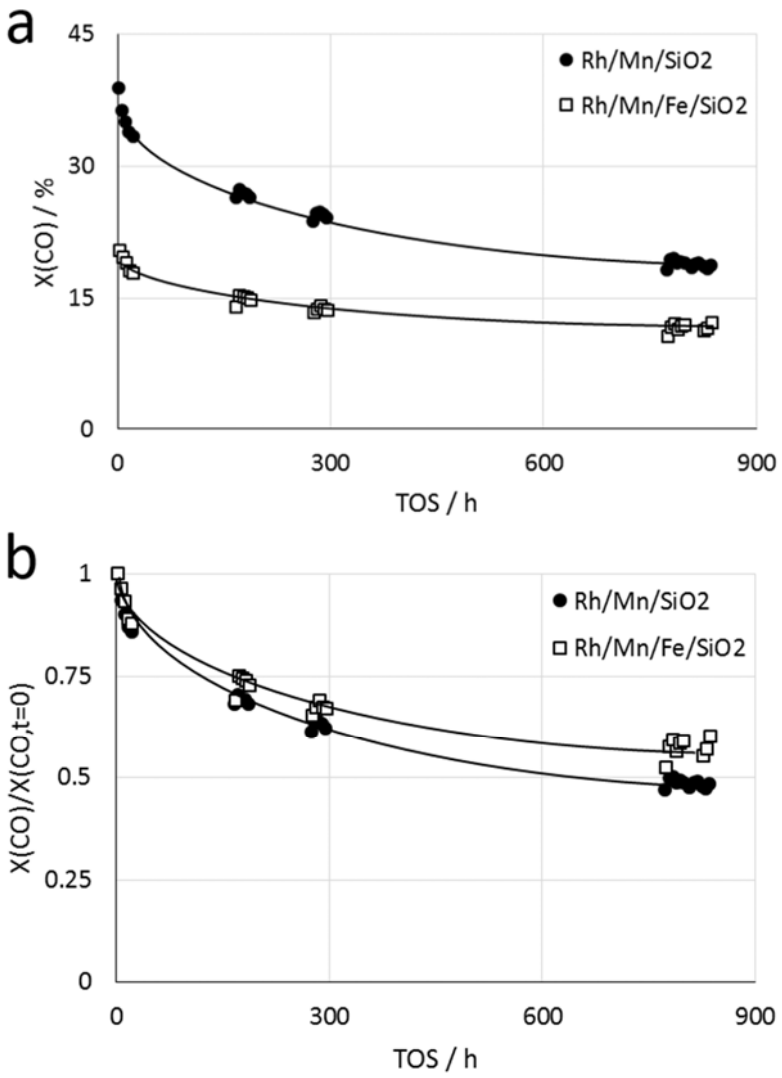

Figure S1. Comparison of Rh-Mn/SiO_2 and Rh-Mn-Fe/SiO_2 in terms of (a) conversion of CO as a function of time on stream (TOS), and (b) conversion of CO as a function of TOS normalized to the initial conversion.

3) XPS Rh3d of calcined Rh-based catalysts.

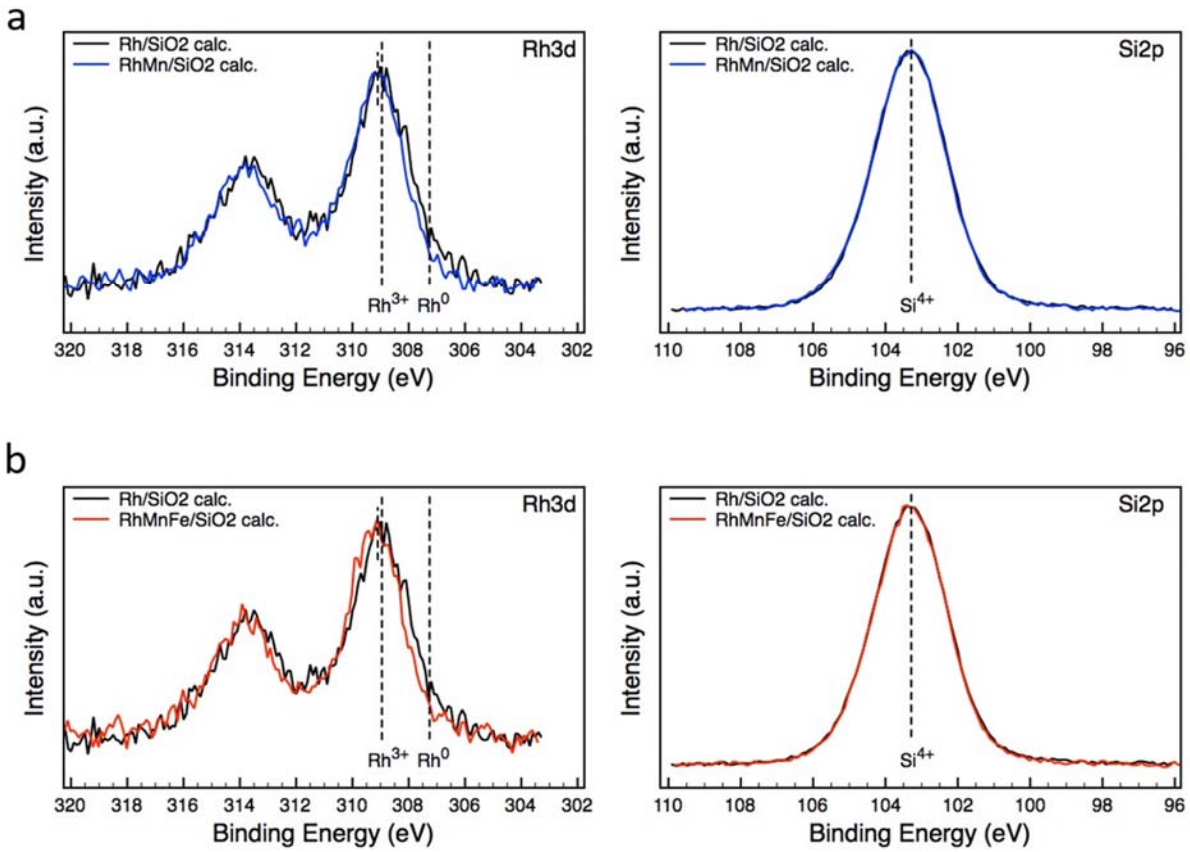

Figure S2. XPS comparison of (a) Rh/SiO_2 (black) and $Rh\text{-}Mn/SiO_2$ (blue); (b) Rh/SiO_2 (black) and $Rh\text{-}Mn\text{-}Fe/SiO_2$ (red) in the calcined state. Left: Rh 3d; right: Si 2p spectra. Si 2p was used as a binding energy reference. Rh 3d is slightly shifted to higher binding energy in both promoted, calcined catalysts compared to that in the unpromoted, calcined Rh/SiO_2. The binding energy shift is indicative of formation of complex $Rh_xMn_yFe_zO_n$ oxides.

4) STEM characterization of unpromoted Rh catalyst in calcined and reduced states.

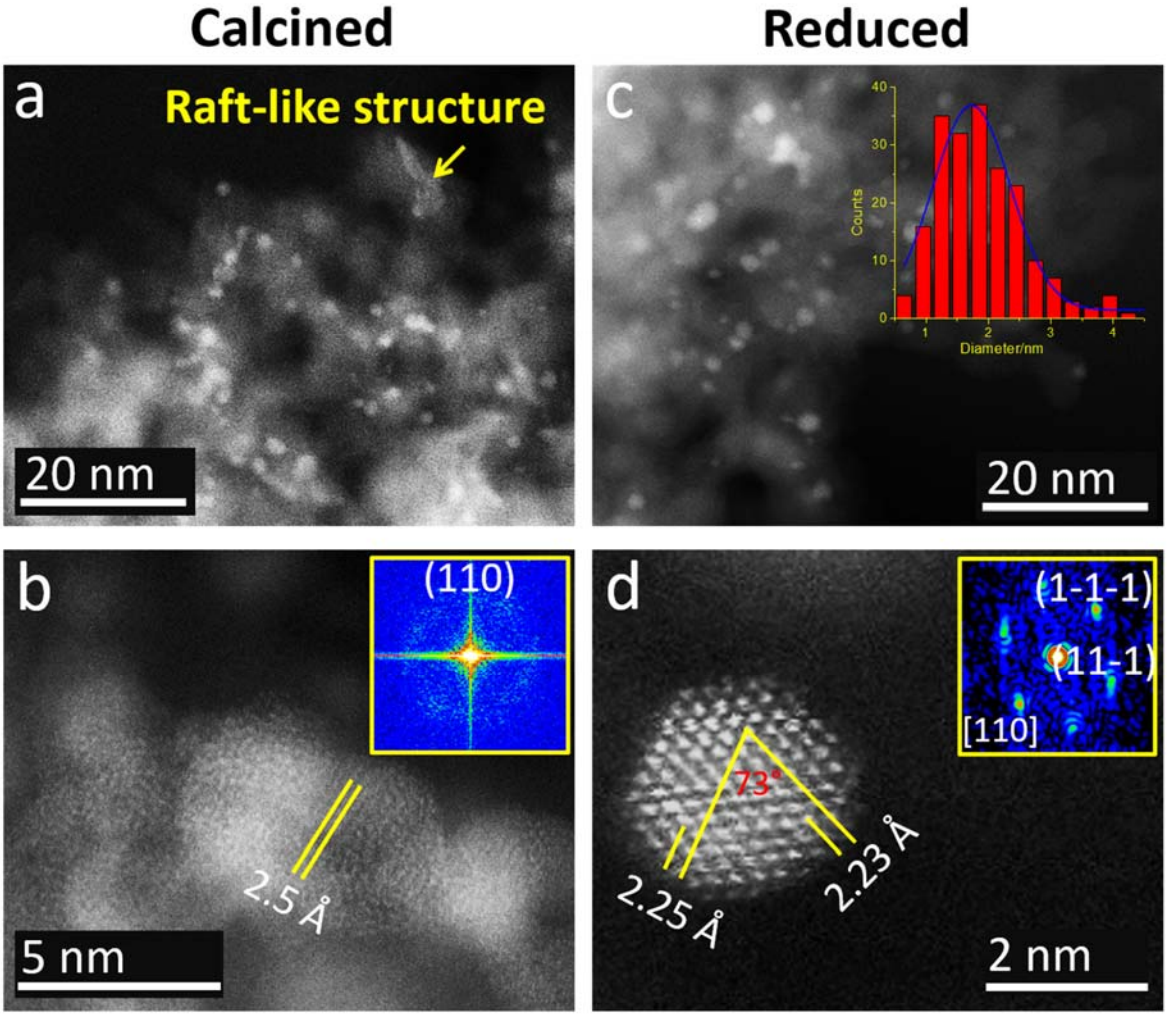

Figure S3. Structural characterization. HAADF-STEM images of (a,b) calcined Rh/SiO_2 and (c,d) reduced Rh/SiO_2 catalyst. Inset of (c) shows particle size dispersion of metallic Rh.

5) STEM and EDX characterizations of calcined Rh-Mn/SiO_2.

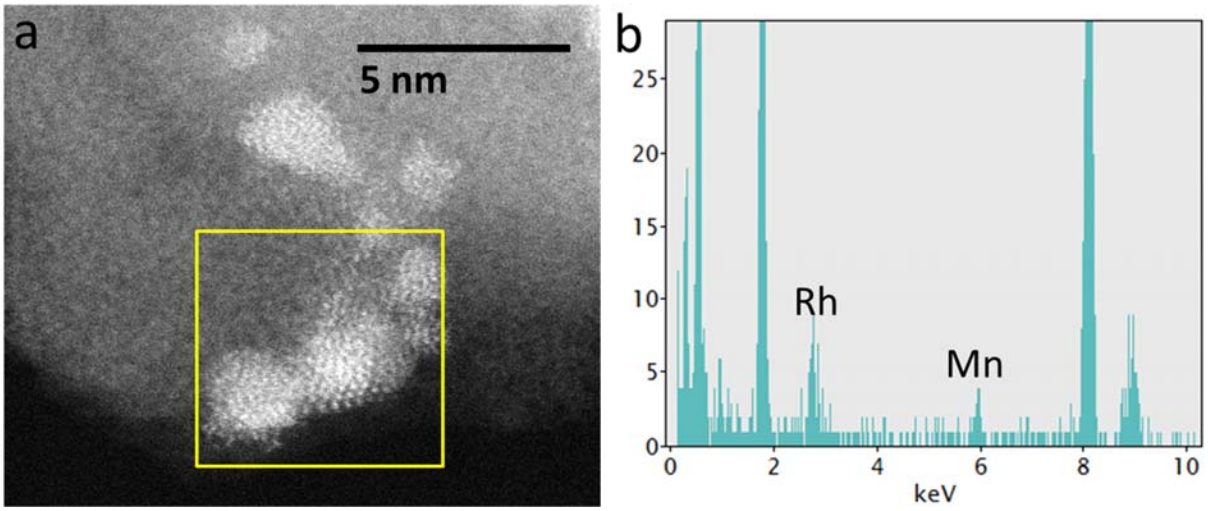

Figure S4. (a) HAADF-STEM image of calcined Rh-Mn/SiO_2 catalyst and (b) EDX spectrum taken from the marked area in (a). EDX analysis from the local particles shows the common presence of Rh and Mn. This finding indicates that Rh_2O_3 and MnO_x are closely contacted or Rh and Mn form complex oxides.

6) STEM and EDX characterizations of calcined Rh-Mn-Fe/SiO_2.

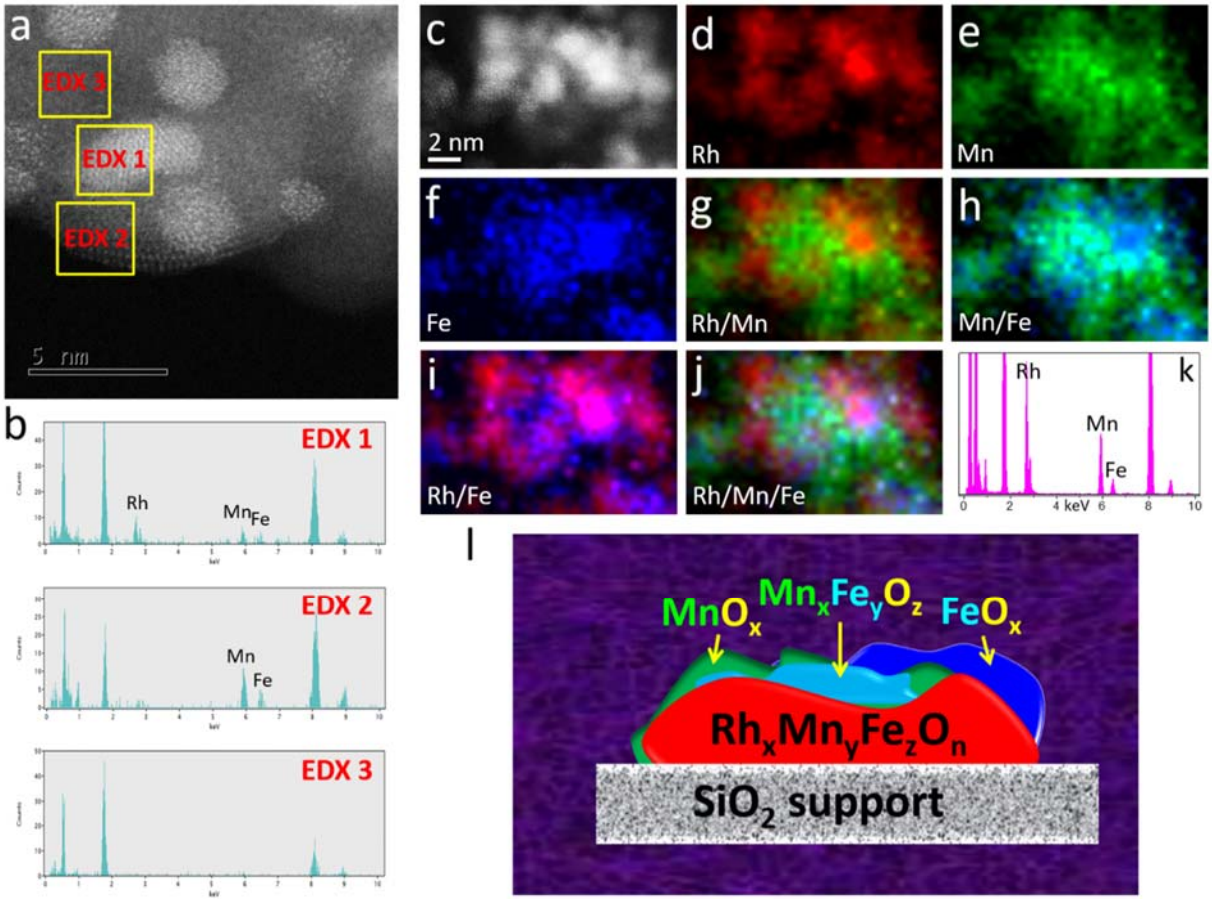

Figure S5. (a) HAADF-STEM image of calcined Rh-Mn-Fe/SiO_2 catalyst; (b) EDX spectra taken from corresponding regions shown in (a); (c-j) HAADF-STEM image of Rh-Mn-Fe/SiO_2 catalyst and corresponding STEM-EDX maps of constituted elements; (k) Summarized EDX spectrum; (l) Schematic model hypothesized for the calcined Rh-Mn-Fe/SiO_2 catalyst.

7) STEM and EDX characterizations of reduced and spent Rh-Mn/SiO_2.

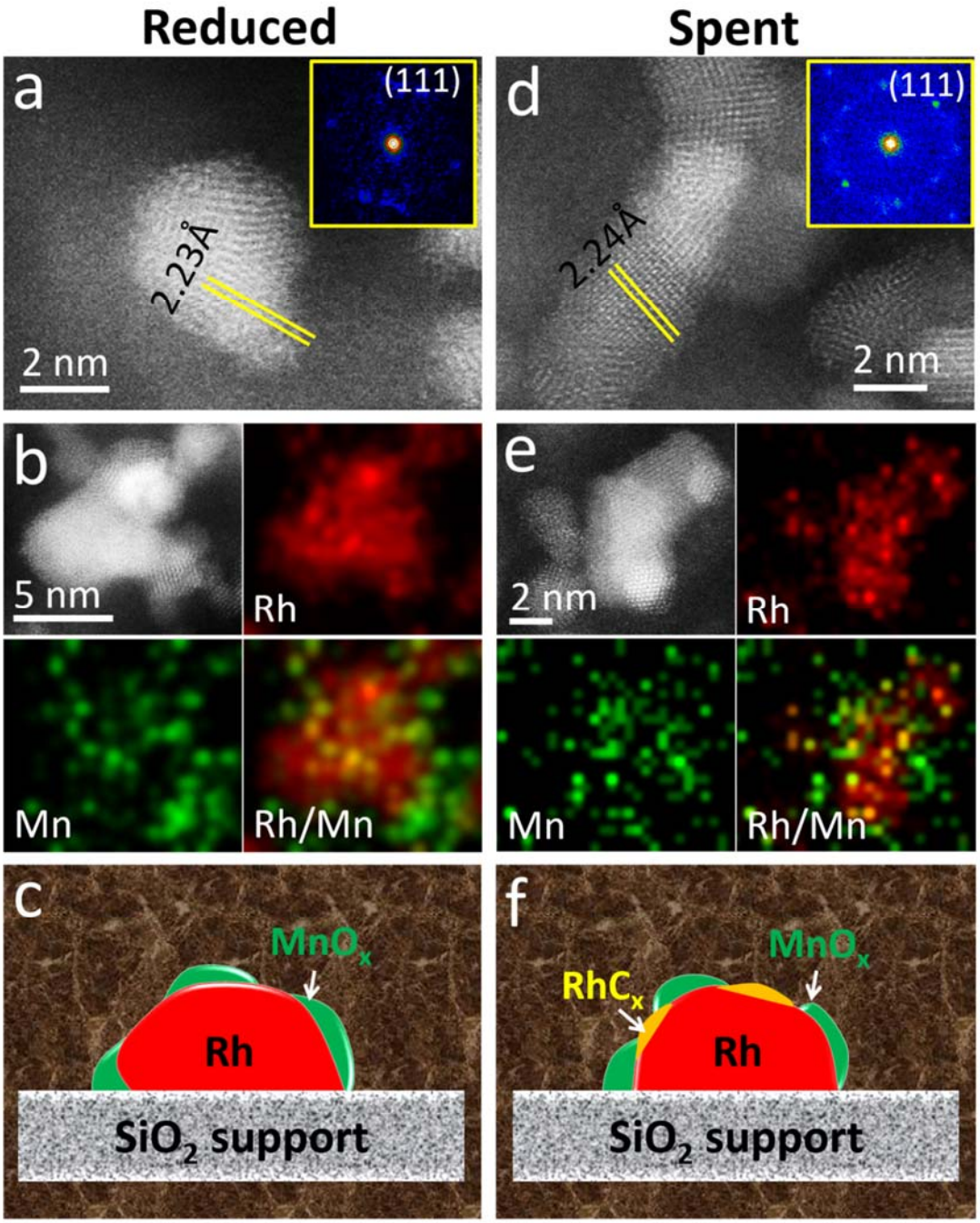

Figure S6. Structural and chemical characterization. HAADF-STEM images of catalytic nanoparticles in (a) reduced and (d) spent Rh-Mn/SiO_2 catalysts; insets show FFTs; (b,e) HAADF-STEM image and corresponding EDX maps; Schematic models of nanoparticles for (c) reduced and (f) spent catalysts, respectively.

Discussion on Figure S6. After reduction and catalytic reaction, most of particles remain small and get reduced to metallic Rh, as shown in Figure S6a and d. The EDX mapping analysis further reveals that Mn signal locates closely around Rh particles. Based on this observation, we propose structural models for catalyst after the reduction and the catalytic reaction (Figure S6c and f). It is a core/shell structure with Rh being partially covered by MnO_x. It is worth mentioning that after long-term reaction big particles with sizes up to 20-40 nm are also formed. The images are shown Figure S9. The sintered particles are characterized by both EDX and EELS, which suggests the formation of RhC_x (see Figure S16,17). Serious sintering occurred as well on Rh-Mn-Fe/SiO_2 catalyst after long-term reaction, please see Figure S10. Instead, the particles are characterized to be Rh-Fe alloy (see Figure 3 in the main text and Figure S11 in SI).

8) STEM characterization of reduced Rh-Mn/SiO_2.

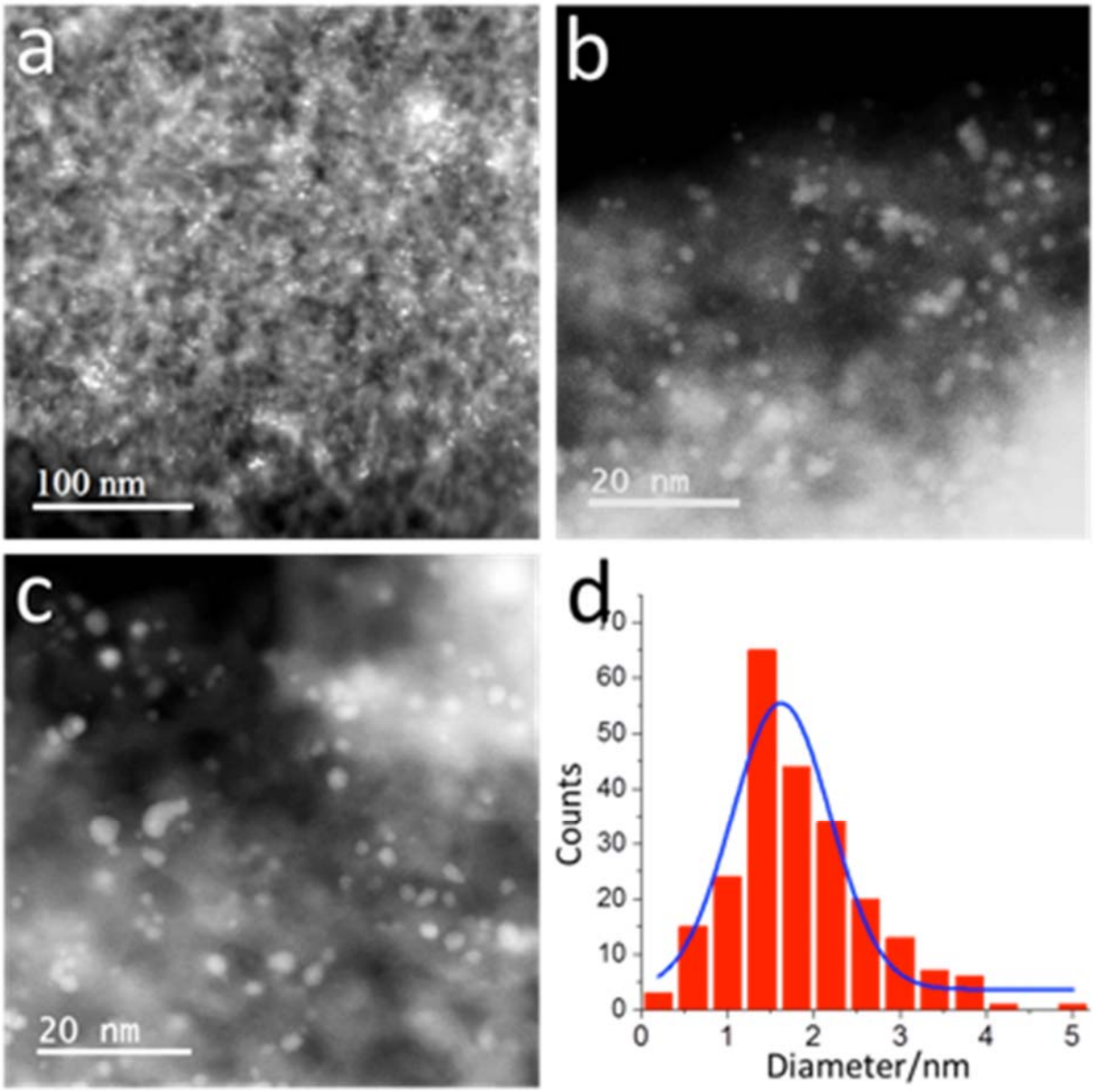

Figure S7. HAADF-STEM images and corresponding particle size distribution of the catalytic particles in reduced Rh-Mn/SiO_2 catalyst.

9) STEM characterization of reduced Rh-Mn-Fe/SiO_2.

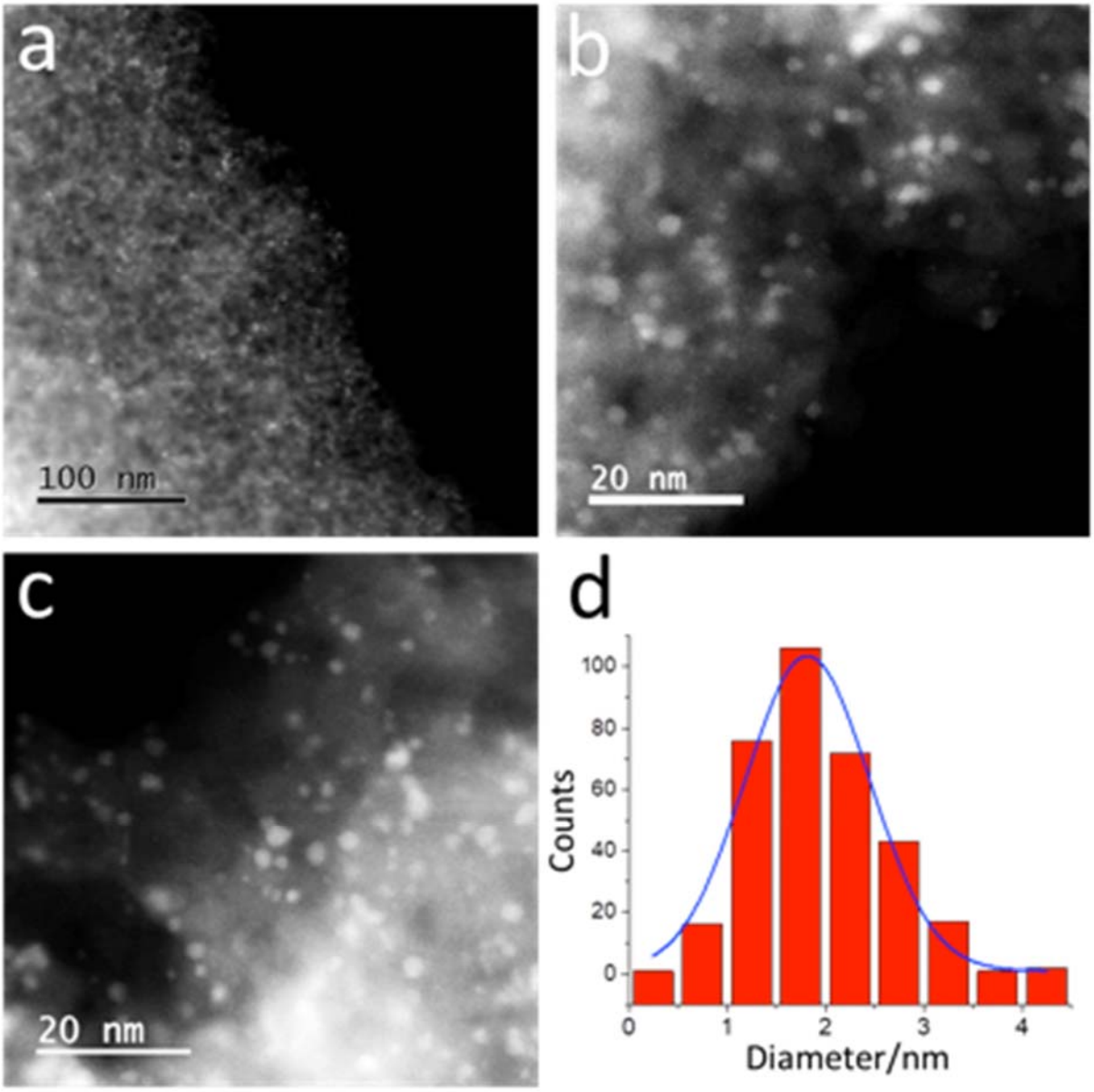

Figure S8. HAADF-STEM images and corresponding particle size distribution of the catalytic particles in reduced Rh-Mn-Fe/SiO_2 catalyst.

10) STEM characterization of spent Rh-Mn/SiO_2.

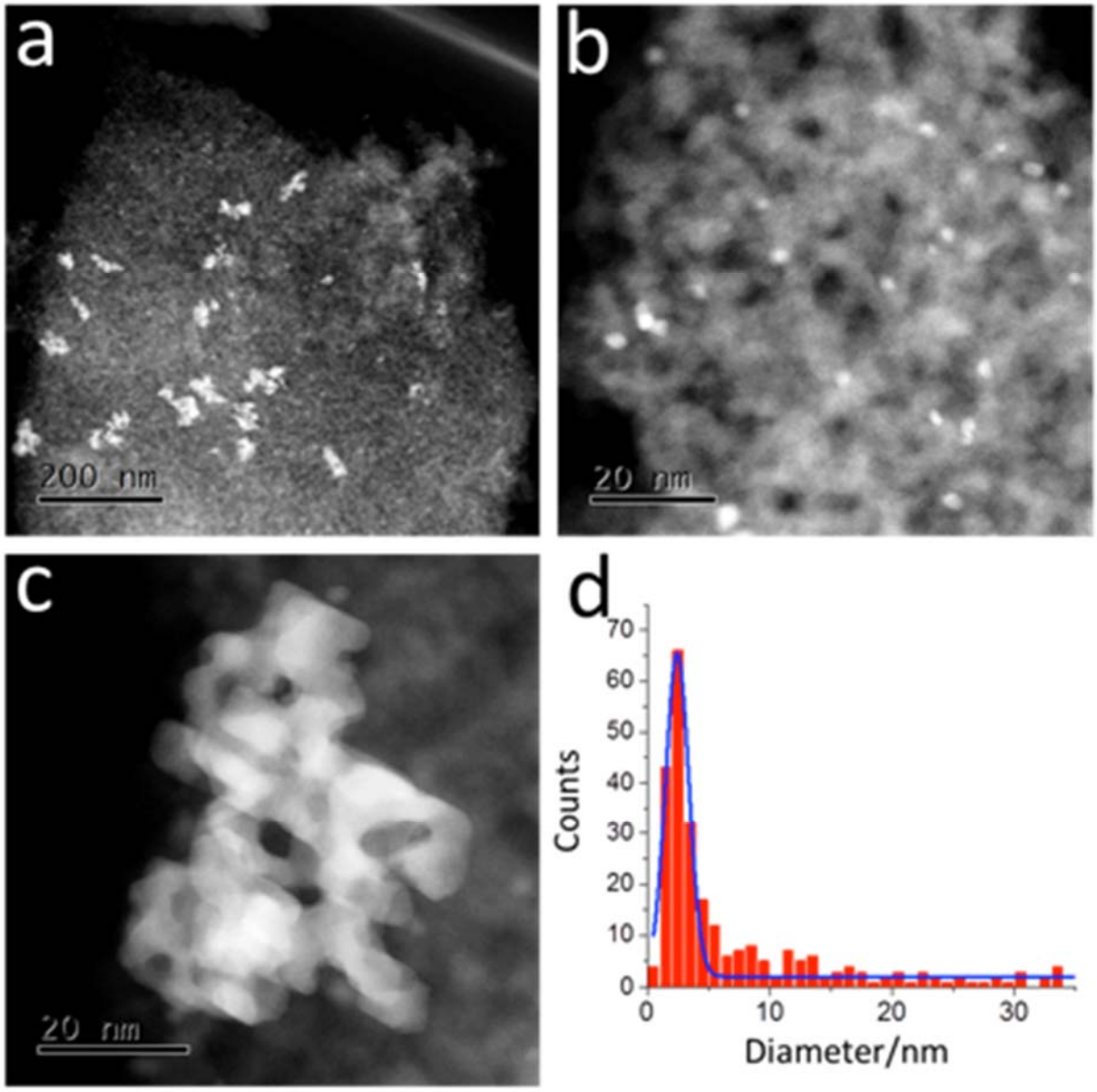

Figure S9. HAADF-STEM images and corresponding particle size distribution of the catalytic particles in spent Rh-Mn/SiO_2 catalyst. With most of particles still showing small size (see Figure S12b), big particles with size up to 40 nm are observed (see Figure S12c).

11) STEM characterization of spent Rh-Mn-Fe/SiO_2.

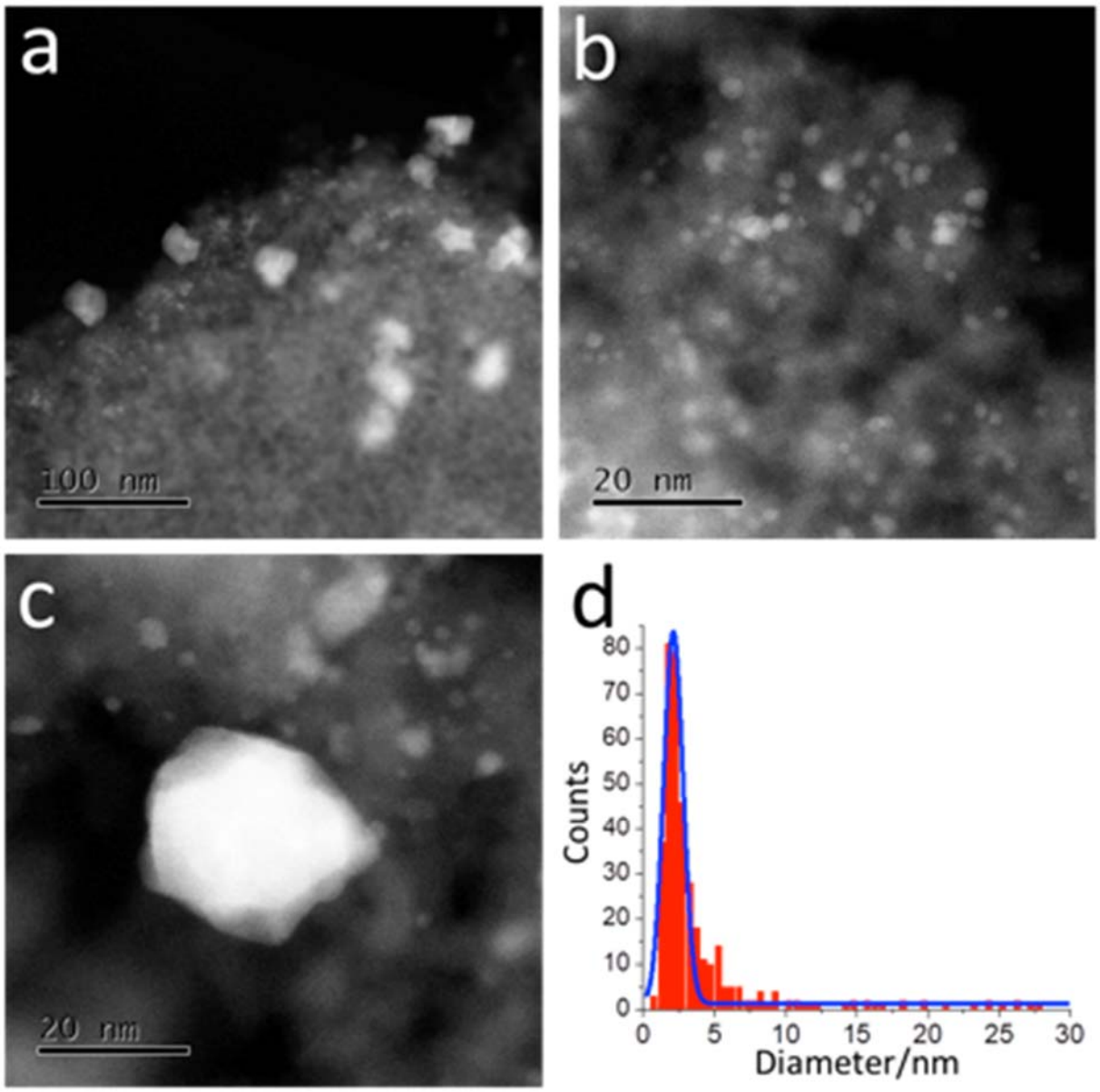

Figure S10. HAADF-STEM images and corresponding particle size distribution of spent Rh-Mn-Fe/SiO_2 catalyst. Although big sized particles appear after reaction (see Figure S13c), most of particles remain small (see Figure S13b), as indicated by the diagram shown in Figure S13d.

12) STEM and EDX characterizations of spent Rh-Mn-Fe/SiO_2.

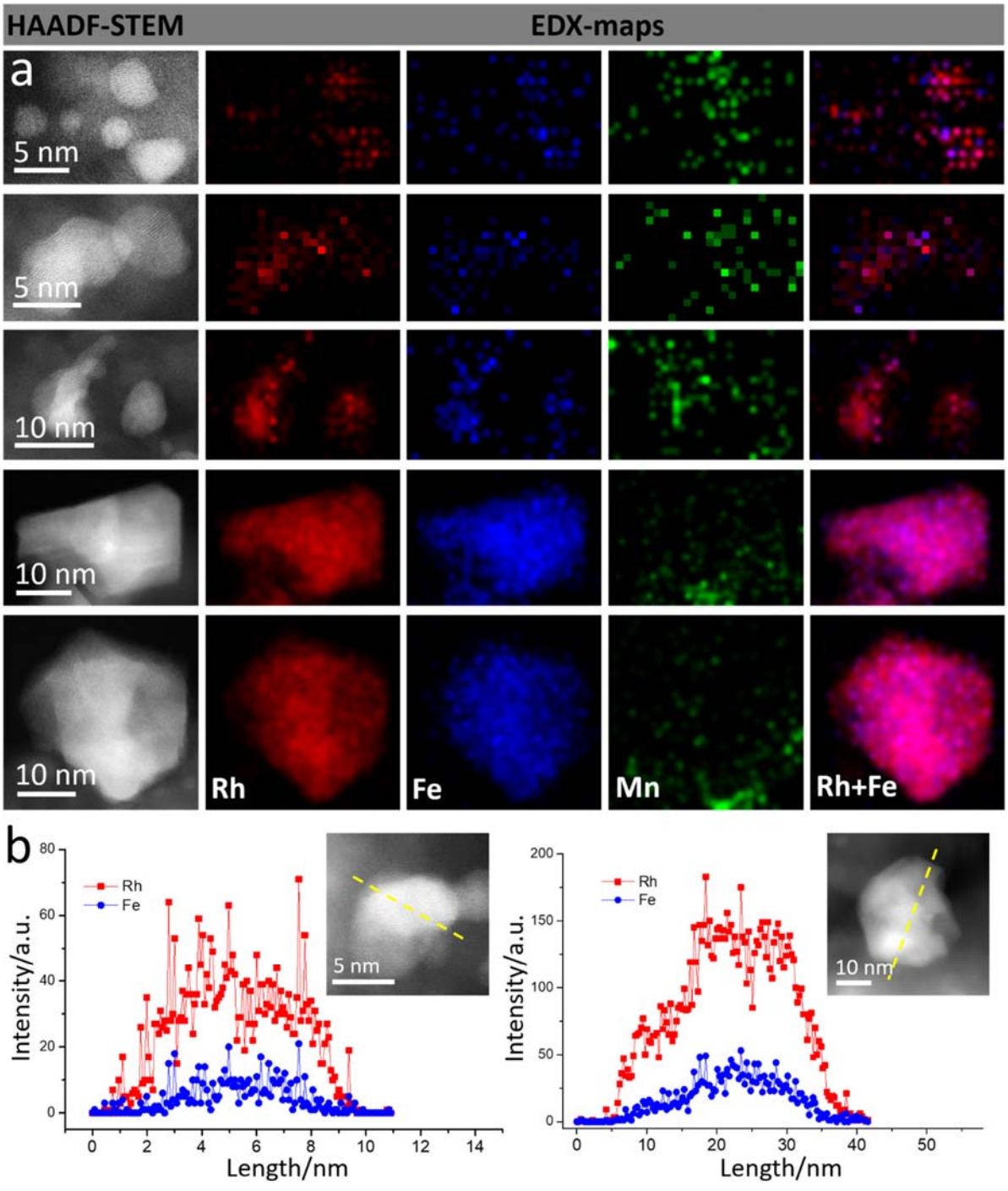

Figure S11. EDX maps and line profiles of catalytic particles with varied sizes in the spent Rh-Mn-Fe/SiO_2, demonstrating the formation of Rh-Fe alloy after catalytic reaction.

13) XPS Rh3d of Rh-based catalysts after reduction and catalytic reaction.

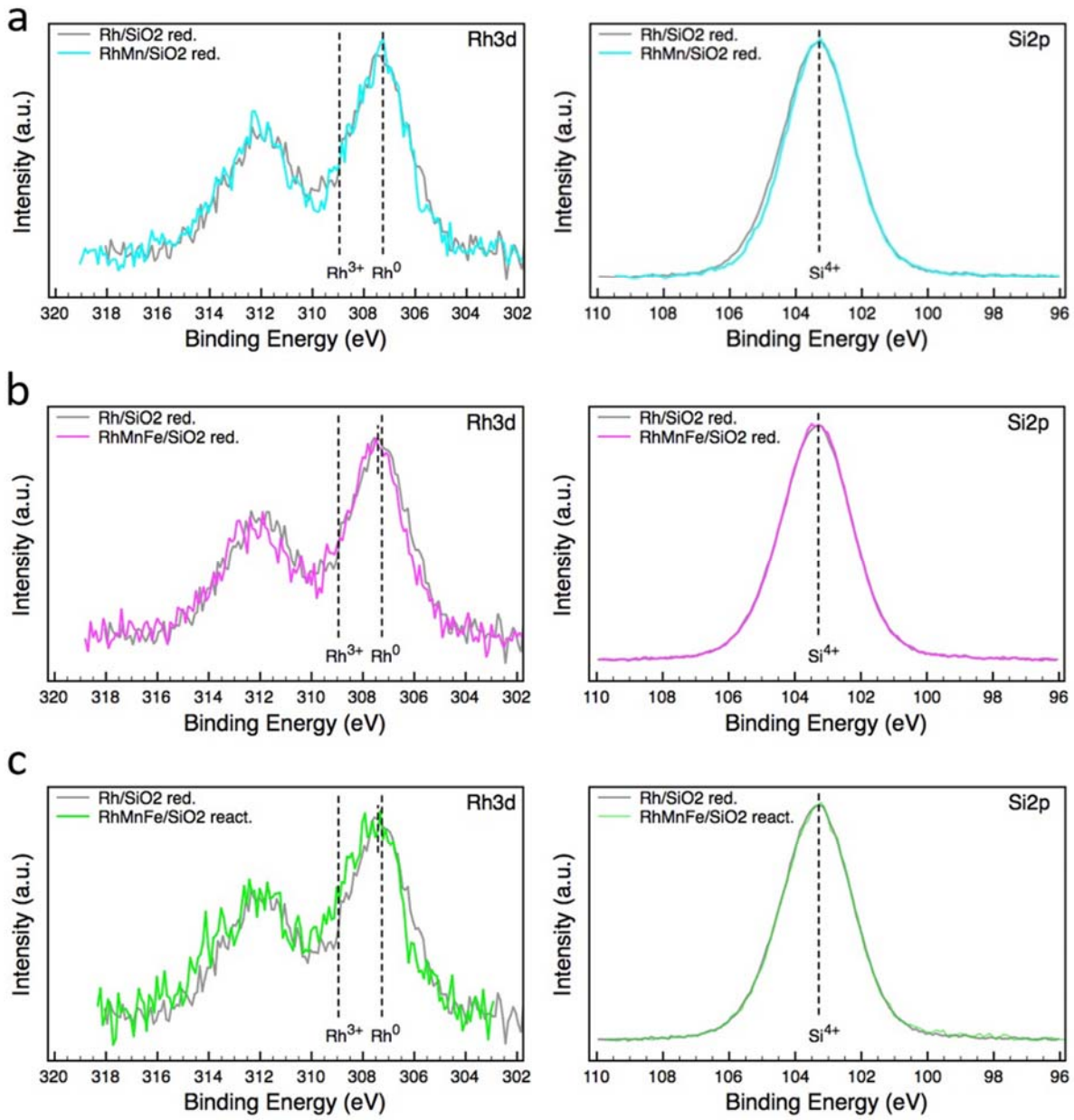

Figure S12. XPS comparison of (a) reduced Rh/SiO_2 and reduced $Rh\text{-}Mn/SiO_2$; (b) reduced Rh/SiO_2 and reduced $Rh\text{-}Mn\text{-}Fe/SiO_2$; (c) reduced Rh/SiO_2 and spent $Rh\text{-}Mn\text{-}Fe/SiO_2$. Left Rh 3d, right Si 2p spectra are shown. Si 2p was used as a binding energy reference.

14) EDX analysis of Rh-Fe alloys in reduced and spent Rh-Mn-Fe/SiO_2.

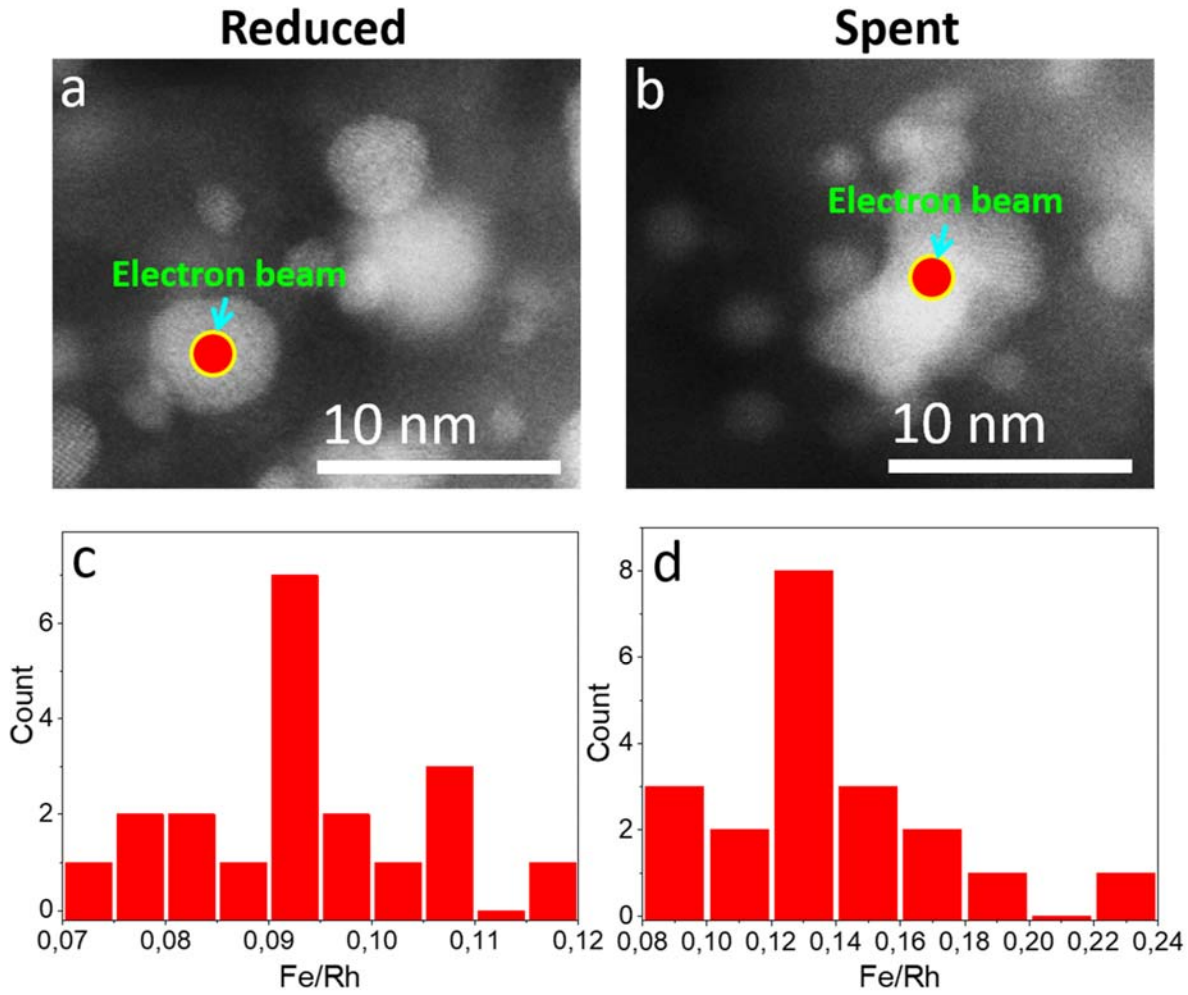

Figure S13. Statistical study on Fe/Rh mass ratio of alloy particles in (a,c) reduced and (b,d) spent Rh-Mn-Fe/SiO_2 catalyst based on EDX-point analysis (For each sample 20 particles were counted). It is estimated that in reduced Rh-Mn-Fe/SiO_2 catalyst, about 48.5% of Fe was incorporated into Rh. This value was increased to about 71.4% in the spent Rh-Mn-Fe/SiO_2 catalyst.

15) STEM-EELS maps of spent Rh-Mn-Fe/SiO_2.

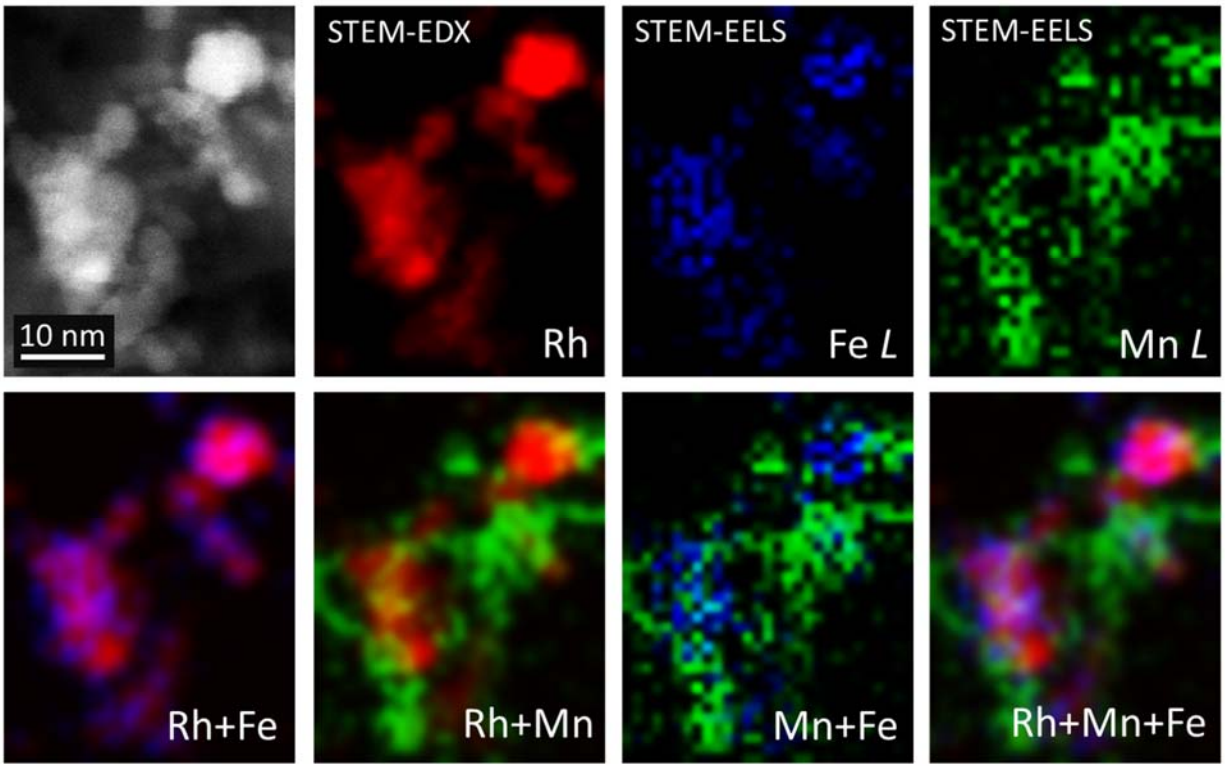

Figure S14. HAADF-STEM image of spent Rh-Mn-Fe/SiO_2 and corresponding STEM-EELS maps (For mapping Rh, EDX signal was used).

16) XPS Mn2p of Rh-Mn-Fe/SiO_2 catalyst in calcined and reduced states.

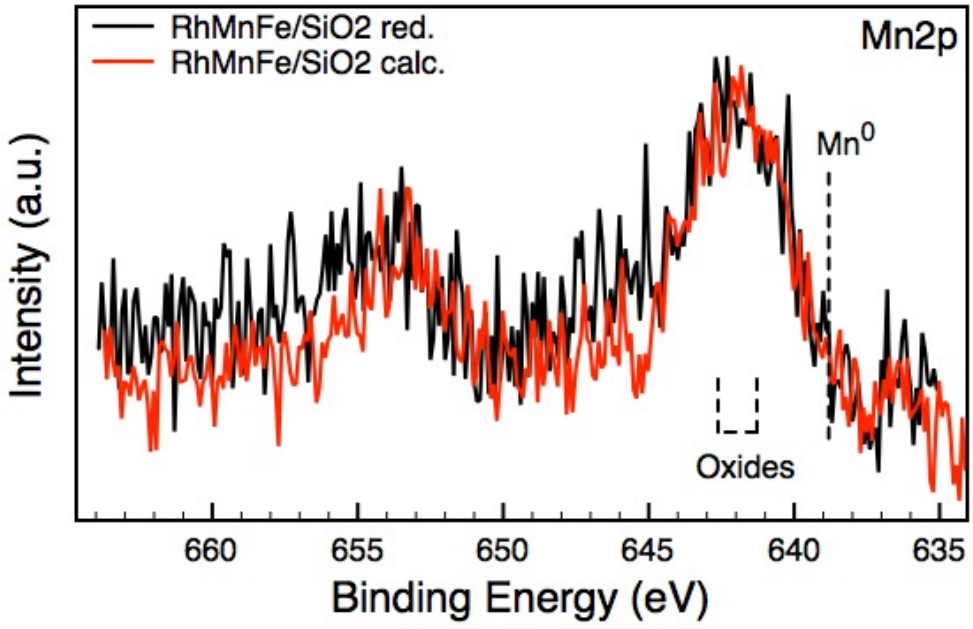

Figure S15. XPS comparison of Rh-Mn-Fe/SiO_2 catalyst in calcined and reduced states. Left: Mn2p after calcination and reduction, right: Rh 3d after reduction and catalytic reaction.

17) STEM-EELS and STEM-EDX maps of Rh carbide in spent Rh-Mn/SiO_2.

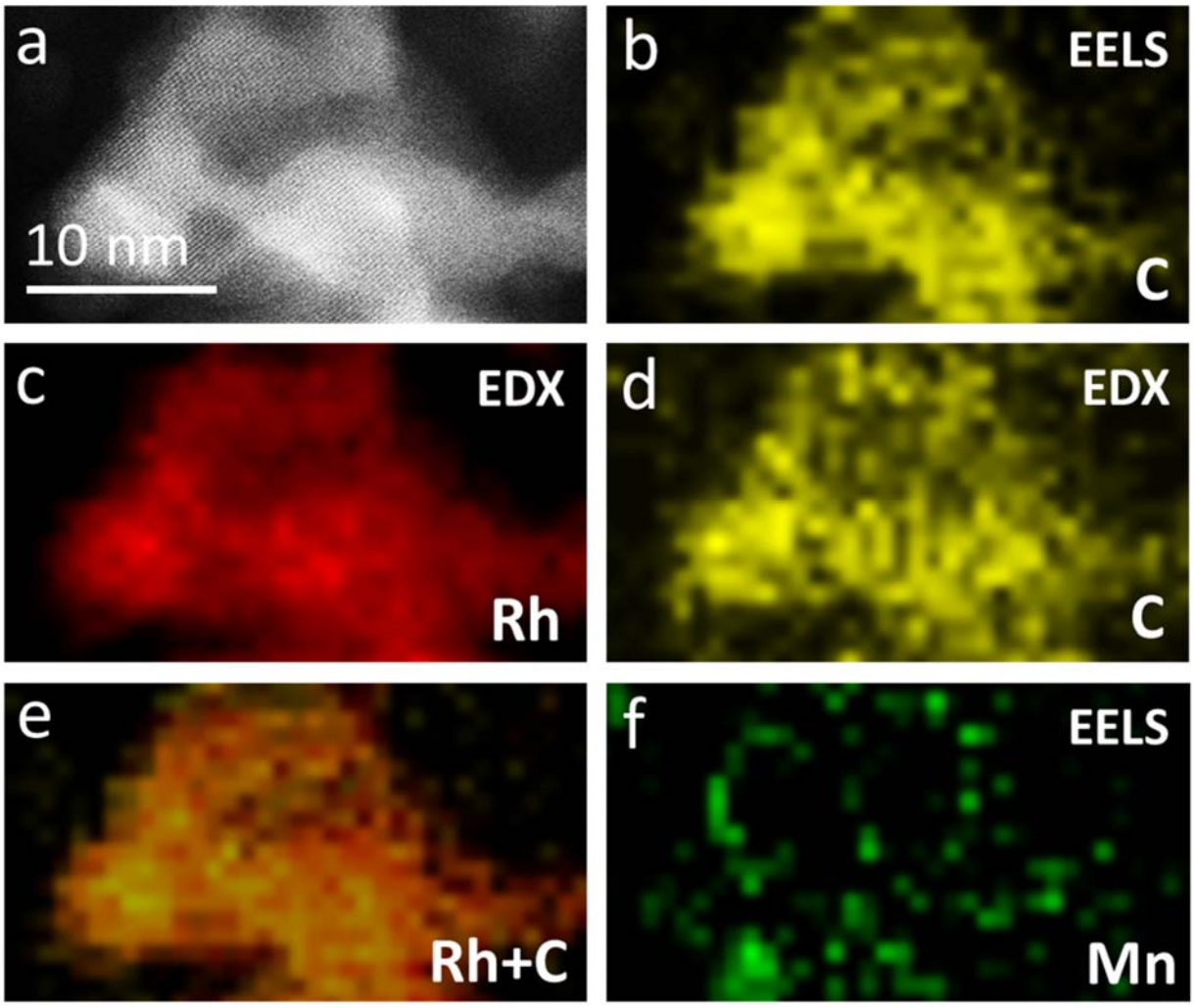

Figure S16. (a) HAADF-STEM image of a sintered particle in the spent Rh-Mn/SiO_2 catalyst; (b) STEM-EELS map of C; (c) EDX map of Rh; (d) EDX map of C; (e) Superimposed map of Rh and C; (f) STEM-EELS map of Mn. The spontaneously recorded STEM-EELS and STEM-EDX maps show a similar distribution of Rh and C, suggesting the formation of RhC_x.

18) STEM-EELS characterization of sintered particles in spent Rh-Mn/SiO_2 and Rh-Mn-Fe/SiO_2.

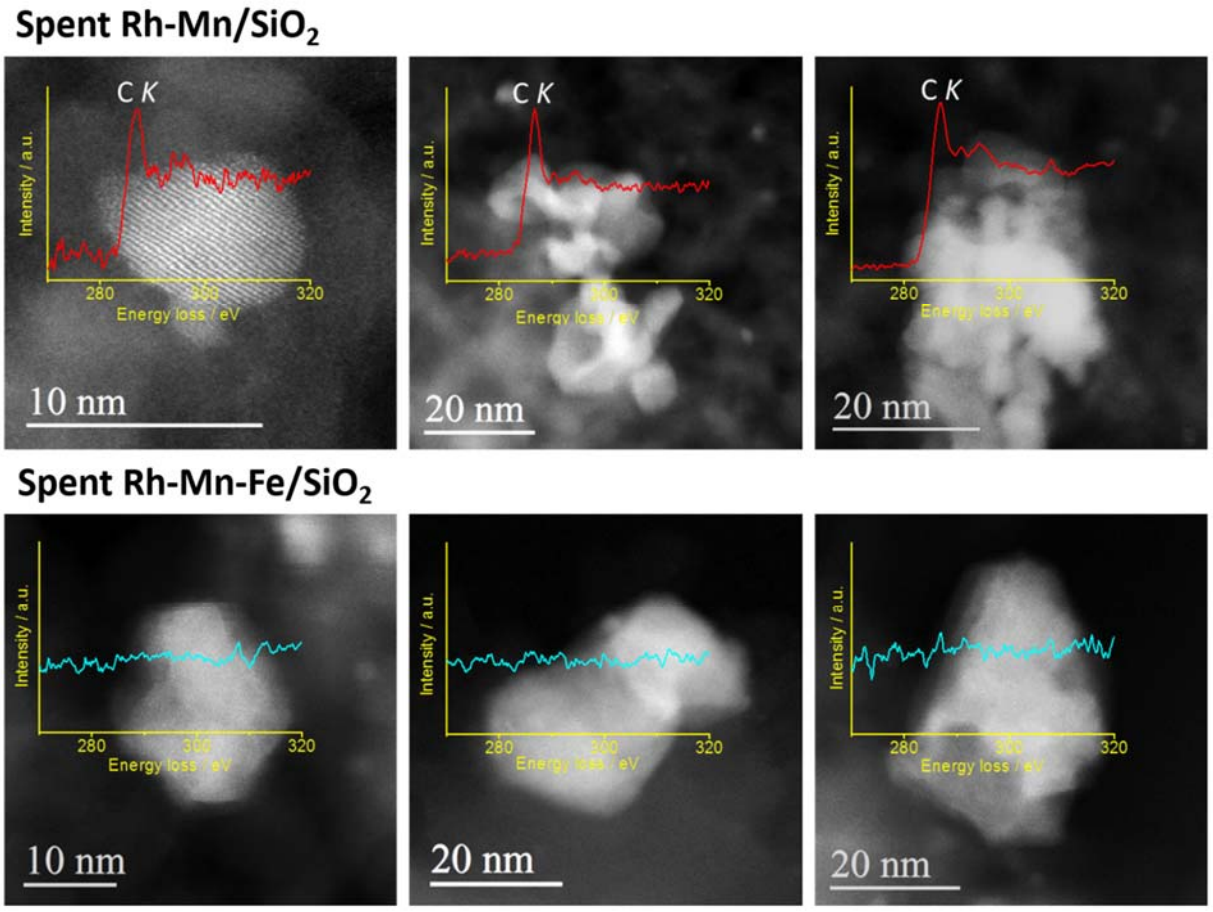

Figure S17. HAADF-STEM images of sintered particles formed in the catalytically spent Rh-Mn/SiO_2 and Rh-Mn-Fe/SiO_2 catalysts and their corresponding EELS spectra in energy range from 270 to 320 eV.

19) STEM-EELS analysis of carbon K edge on small nanoparticles in spent Rh-Mn/SiO_2.

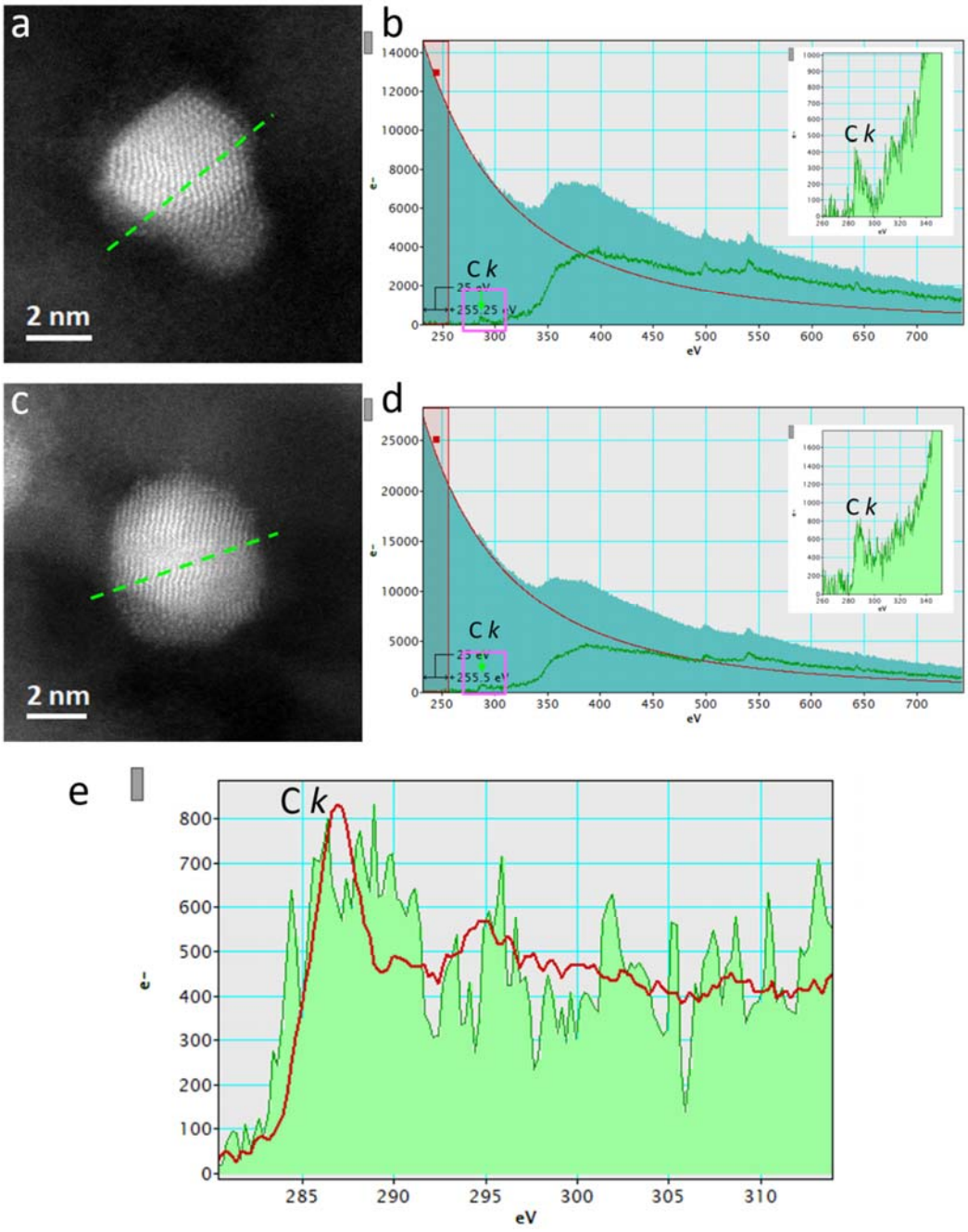

Figure S18. (a,c) HAADF-STEM images of small nanoparticles in spent Rh-Mn/SiO_2 and (b,d) the corresponding EELS-line scans; (e) Comparison of carbon *K* edge recorded from small nanoparticles and RhC_x particles. The carbon *K* edges from both show very similar feature, indicating formation of sub-surface RhC_x on small nanoparticles.

20) XPS Rh3d of reduced Rh/SiO_2 and spent $Rh\text{-}Mn/SiO_2$ catalysts.

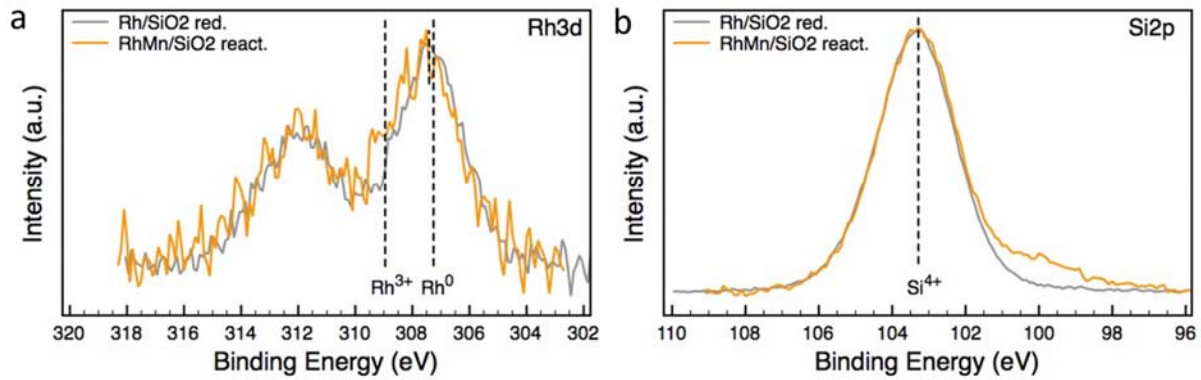

Figure S19. XPS comparison of Rh3d in reduced Rh/SiO_2 and spent $Rh\text{-}Mn/SiO_2$ catalysts.